Volume 55
Number 7
17 February 2026
Pages 2731-3154

Dalton Transactions

An international journal of inorganic chemistry

rsc.li/dalton

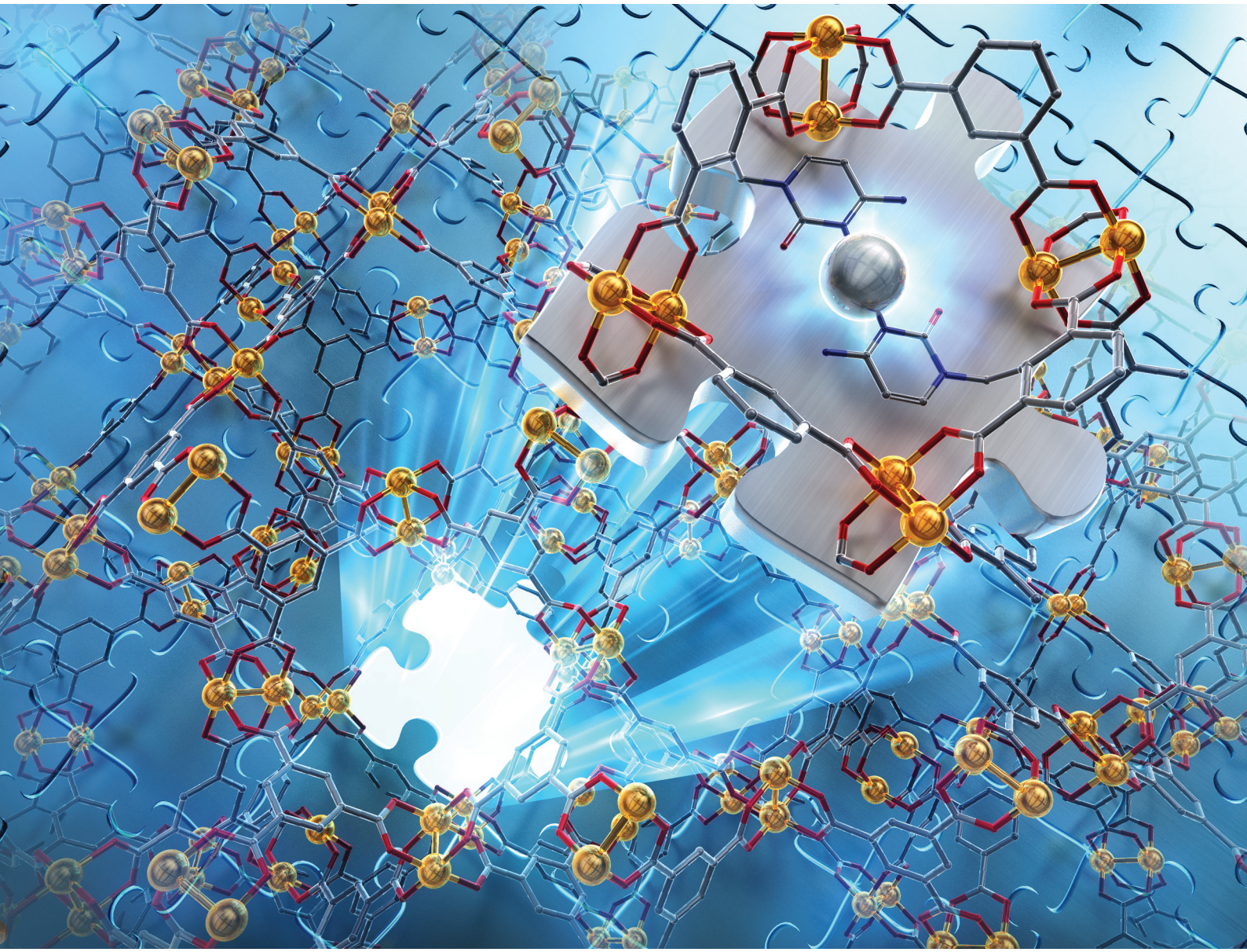

ISSN 1477-9226

ROYAL SOCIETY OF CHEMISTRY

PAPER

Youngjo Kim, Soyoung Park, Min Kim *et al.*
A cytosine–silver incorporated metal–organic framework for efficient laccase-mimicking reactions

Dalton Transactions

ROYAL SOCIETY OF CHEMISTRY

PAPER

View Article Online
View Journal | View Issue

Cite this: *Dalton Trans.*, 2026, **55**, 2817

A cytosine–silver incorporated metal–organic framework for efficient laccase-mimicking reactions

Jonghyeon Lee, [a] Gahyeon Baek, [a] Youngjo Kim, *[a] Soyoung Park *[b] and Min Kim *[a]

Received 27th November 2025,
Accepted 18th December 2025

DOI: 10.1039/d5dt02837j

rsc.li/dalton

Nucleobases are essential components of nucleic acids and provide multiple coordination sites, making them useful ligands for metal-based catalysis. Purine-type nucleobases such as adenine and guanine have been widely studied because of their rigid structures and strong metal-binding ability, whereas the pyrimidine-type cytosine (Cyt) has seen far less use in catalysis. Here, we present a new catalyst: a Cu-based metal–organic framework (MOF) modified with the biocompatible nucleobase Cyt. Silver ions are chelated by the Cyt–Ag structure inside the MOF, forming a bimetallic nanozyme named HKUST-1-Cyt–Ag (HKUST = Hong Kong University of Science and Technology). This hybrid exhibits strong laccase-like activity, driven by the synergy between the Cu-based HKUST-1 framework and the Cyt–Ag motif. To our knowledge, this is the first demonstration of ligand-chelating metalation in HKUST-1, highlighting its potential to mimic multicopper oxidase activity for biocatalytic applications.

Introduction

Nucleobases are nitrogen-rich heterocyclic biomolecules that serve as the fundamental building blocks of nucleic acids such as DNA and RNA.[1,2] In nucleic acids, nucleobases play a unique role by forming complementary base pairs through hydrogen-bonding interactions—most notably Watson–Crick base pairing—thereby contributing to the formation of the double helix structure. Beyond hydrogen bonding, the nitrogen- and oxygen-rich structures of nucleobases allow coordination bonding with various metal ions, making them widely utilized as ligands in bioinorganic complexes. In particular, nucleobases complexed with catalytically active metals have been reported to act as effective catalysts in a variety of organic and biochemical reactions.[3,4]

Purine-based nucleobases such as adenine (Ade) and guanine (Gua) possess multiple coordination sites and have therefore been widely employed for the construction of metal complexes, whereas the pyrimidine-based analogues like thymine (Thy) and cytosine (Cyt) offer relatively fewer coordination sites and have received much less attention.[4–6] A broad range of metal–purine complexes have been developed for catalytic applications, while analogous Cyt-based catalytic systems remain extremely rare. This imbalance is clearly reflected in the comprehensive review by Nikoofar and coworkers, who surveyed metal–nucleobase-based catalysts and identified 33 catalytic systems for purine-based nucleobases, but only 6 catalytic examples for pyrimidine nucleobases. This pronounced discrepancy highlights that Cyt-based catalytic systems remain significantly underexplored compared to their purine counterparts.

In particular, existing studies on metal–Cyt complexes focus on only a few isolated catalytic examples, underscoring the lack of a systematic framework for Cyt-based catalysis. Recently, the Hajjami group and the Nikoorazm group independently immobilized Cyt–Pd and Cyt–Ni complexes on mesoporous silica supports and applied them to organic transformations (Fig. 1a).[7,8] These isolated examples, however, represent rare exceptions within an otherwise sparsely developed field. Meanwhile, we developed modular DNA hybrid catalysts and demonstrated that Cyt exhibits distinct behavior compared to other nucleobases.[9] Based on this observation, we constructed a Cu-based DNA hybrid catalyst system that functions without conventional ligands (*e.g.*, bipyridine or phenanthroline), incorporating a Cyt–Cu complex within the DNA duplex as the catalytic center. This system exhibited high activity and enantioselectivity in asymmetric Diels–Alder reactions, providing a representative study where Cyt functions as an effective coordinating ligand for metal-catalyzed organic reactions.[10]

At the oligonucleotide level, structural changes and stabilization effects induced by metal–pyrimidine interactions have also highlighted the untapped potential of this area. Among

[a]*Department of Chemistry, Chungbuk National University, Cheongju, 28644, Korea. E-mail: ykim@chungbuk.ac.kr, minkim@chungbuk.ac.kr*
[b]*Immunology Frontier Research Center, The University of Osaka, Osaka, 565-0871, Japan. E-mail: spark@ifrec.osaka-u.ac.jp*

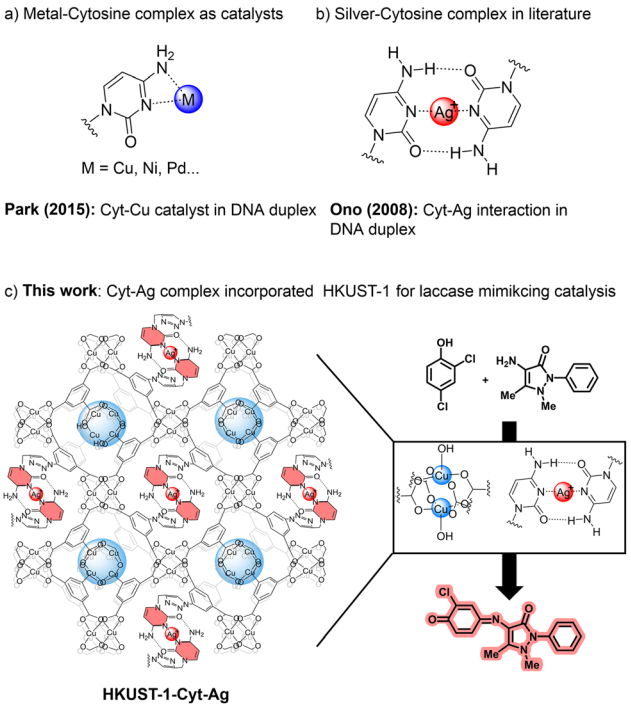

Fig. 1 Cytosine incorporated HKUST-1 for laccase-mimicking catalysis. (a) Reported metal–cytosine complex catalysts. (b) Previous silver–cytosine complex in the literature. (c) Synergistic laccase-mimicking performance of the Cu cluster and Cyt–Ag motif in HKUST-1-Cyt–Ag.

these, Cyt–Ag complexes are particularly well known for their strong interactions between Ag(I) ions and Cyt, affording thermodynamically stable structures. In 2008, Ono *et al.* reported that Cyt–Ag–Cyt complexes in DNA duplexes exhibited enhanced thermal stability compared with pristine DNA (Fig. 1b).[11] Kondo and co-workers developed Ag–DNA hybrid nanowires, with their structures elucidated by X-ray crystallography.[12] Cyt-rich i-motif structures have also served as useful scaffolds for visualizing metal–base interactions (Fig. 1b).[13] In catalytic applications, recent studies have reported that the unique binding affinity of the Cyt–Ag array confers enhanced stability and efficiency in heterogeneous platforms such as DNA hybrid catalysts, metal nanoparticles and covalent organic frameworks (COFs).[14–16] Despite these developments, no Cyt–Ag-based catalyst has yet been demonstrated to work effectively in well-established Ag(I)-catalyzed reactions.[17–21] To make full use of the Cyt–Ag system's properties, it must be integrated into a solid support, and the incorporation and function of Cyt–M–Cyt species in a robust catalytic platform should be examined in detail.

Metal–organic frameworks (MOFs) are well-defined, crystalline hybrid materials, which are composed of inorganic metal clusters and multi-topic organic linkers. The structural tunability of MOFs, arising from the diverse combinations of metal nodes and organic linkers, enables the rational design of a wide spectrum of framework architectures and target-oriented applications including gas separation, sensing and catalysis.[22–26] In particular, recent applications of MOFs have moved toward bio-related fields, and a wide range of biomolecules and bioactive species have been incorporated into MOFs.[27–30] In this context, we devised a system to incorporate Cyt–Ag complexes into MOFs to achieve stable immobilization and controlled coordination. Among various metal-based MOF systems, Cu-based HKUST-1 (HKUST = Hong Kong University of Science and Technology) MOFs were selected as the main platform because Cu has been widely studied for DNA catalysis.[9,10,14] HKUST-1 is one of the most well-studied MOFs in the literature and shows good stability and processability compared to other MOFs.[31–33] HKUST-1 is built from Cu(II)-based paddle-wheel secondary building units (SBUs) and a tridentate 1,3,5-benzenetricarboxylate (BTC) ligand. Moreover, the catalytic activity and applications of HKUST-1 itself have been widely explored for various catalytic reactions.[34–36]

Here, we introduce Cyt–Ag species into Cu-based HKUST-1 by anchoring Cyt onto the MOF ligand, followed by post-metalation, producing HKUST-1-Cyt–Ag for laccase-mimicking reactions (Fig. 1c). The hybrid material combines the structural stability of HKUST-1 with the catalytic properties of Cyt–Ag, showing strong activity in laccase-like oxidation and offering new possibilities for MOF-based nanozymes in biocatalysis and environmental applications.

Results and discussion

Synthesis of HKUST-1-Cyt–Ag

Cu-based HKUST-1 was synthesized under solvothermal conditions from $Cu(NO_3)_2$ and H_3BTC in an *N*,*N*-dimethylformamide (DMF)–ethanol–water co-solvent system. By exchanging the H_3BTC ligand with a functionalized ligand, the desired functionality could be installed into the HKUST-1 MOF. Because H_3BTC contains only sterically hindered positions on its benzene ring, Cyt incorporation was performed at the 5-position of isophthalic acid (benzene-1,3-dicarboxylic acid, *meta*-benzene dicarboxylic acid, H_2*m*BDC). Mixed-ligand systems composed of H_3BTC and functionalized H_2*m*BDC have been widely explored to prepare functionalized HKUST-1.[37] The direct connection of Cyt to H_2*m*BDC was achieved *via* a Cu-catalyzed alkyne–azide cycloaddition reaction through a triazole moiety (Scheme S1, SI). The molecular structure of H_2*m*BDC–Cyt was confirmed by nuclear magnetic resonance (NMR), infrared (IR) spectroscopy, and high-resolution mass spectrometry (HRMS).

Next, HKUST-1 was synthesized using the target ligand H_2*m*BDC–Cyt under solvothermal conditions. Owing to the steric hindrance of the H_2*m*BDC–Cyt ligand and structural defects caused by replacing the tricarboxylate linker with a dicarboxylate one, the ligand mixing ratio was adjusted, as shown in Scheme 1. The incorporation ratio of H_2*m*BDC–Cyt was successfully controlled between 10% and 40% during solvothermal synthesis (Fig. 2). Crystalline MOF formation was not achieved when the H_2*m*BDC–Cyt loading exceeded 50%.

Powder X-ray diffraction (PXRD) patterns of all HKUST-1-$(Cyt)_x$ samples fully matched the simulated patterns from the

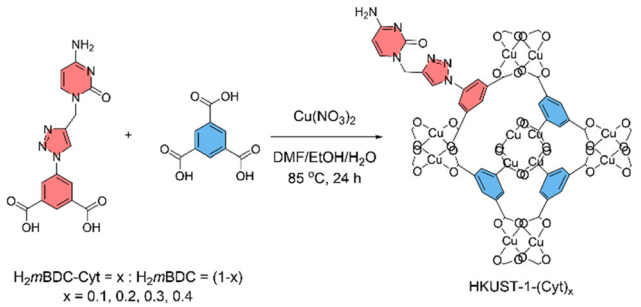

Scheme 1 Synthesis of HKUST-1-(Cyt)$_x$ under various mixed ligand conditions. The ratio of H_2mBDC-Cyt was 10/20/30/40%.

crystal structure of pristine HKUST-1, confirming that the structure of HKUST-1-Cyt was identical to that of pristine HKUST-1 (Fig. 2a). Successful target ligand incorporation was confirmed by ^{1}H NMR data after MOF digestion in acidic solution. The ratio between H_3BTC and H_2mBDC-Cyt matched the mixing ratio used for solvothermal synthesis (Fig. 2b). In addition, the porosity of HKUST-1-(Cyt)$_x$ was examined through N_2 adsorption experiments at 77 K. Generally, the porosity and Brunauer–Emmett–Teller (BET) surface area decreased with increasing H_2mBDC-Cyt ligand ratio in the HKUST-1 MOF (Fig. 2c and Table S1). Furthermore, thermogravimetric analysis (TGA) confirmed that HKUST-1-(Cyt)$_x$ exhibits thermal stability comparable to that of pristine HKUST-1. The DTG curves clearly indicate that HKUST-1-Cyt undergoes framework decomposition at 320–330 °C, slightly lower than the decomposition temperature of pristine HKUST-1 (≈340 °C). This minor decrease is attributed to the increased defect sites introduced by the H_2mBDC-Cyt ligand (Fig. S1).

Subsequently, Ag metalation of HKUST-1-Cyt was carried out using a post-synthetic modification (PSM) approach. HKUST-1-Cyt was treated with an Ag(I)-containing acetonitrile solution for 48 h. The resulting Ag-installed HKUST-1-(Cyt)$_x$–Ag was isolated by simple centrifugation and showed retained crystallinity in PXRD patterns (Fig. 3a). A relative decrease in peak intensity was observed for HKUST-1-(Cyt)$_{0.4}$–Ag, which likely reflects the abundance of defect sites in HKUST-1-(Cyt)$_{0.4}$. Furthermore, scanning electron microscopy coupled with energy-dispersive spectroscopy (SEM-EDS) mapping of HKUST-1-(Cyt)$_{0.3}$–Ag confirmed the uniform distribution of Cu, N, and Ag throughout the MOF sample, indicating that the Cyt ligand and Ag metal were not aggregated within the framework (Fig. 3b). The exact Ag content in HKUST-1-(Cyt)$_x$–Ag was quantified by inductively coupled plasma optical emission spectrometry (ICP-OES). The experimental ICP-OES values were in good agreement with the predicted Ag wt% based on the chemical formula of HKUST-1-Cyt–Ag (Table S2). The Ag loading in the MOFs increased with the increasing content of the Cyt ligand, and the experimental data closely matched the values calculated from the Cyt–Ag–Cyt coordination ratio.

To more clearly confirm the coordination between Ag(I) ions and cytosine, we conducted high-resolution X-ray photoelectron spectroscopy (XPS) analysis targeting the direct

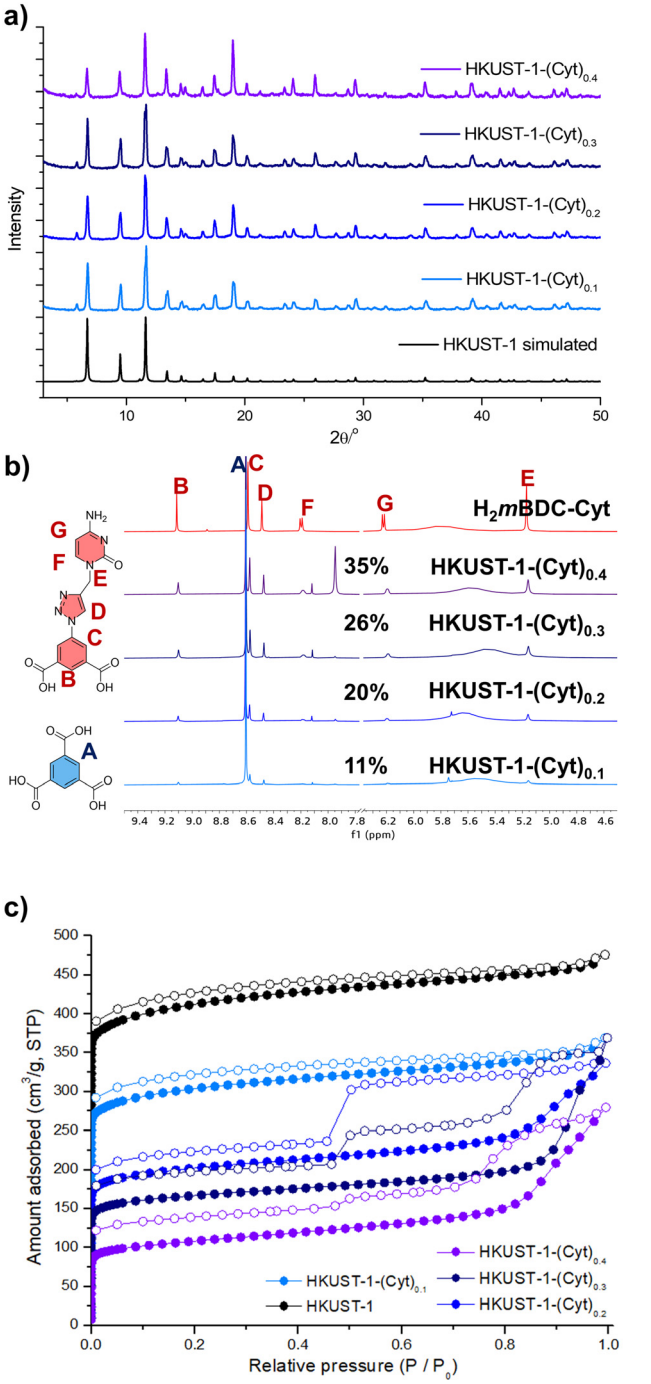

Fig. 2 Characterization data of HKUST-1-(Cyt)$_x$. (a) PXRD of HKUST-1-(Cyt)$_x$, (b) ^{1}H NMR of HKUST-1-(Cyt)$_x$ after acid digestion, and (c) N_2 isotherm at 77 K for HKUST-1-(Cyt)$_x$.

binding sites within the MOF. In the N 1s spectra, the HKUST-1-(Cyt)$_x$–Ag samples exhibited a slight increase in binding energy compared to their corresponding HKUST-1-(Cyt)$_x$ samples (Fig. S2 and Table S3). This shift is consistent with electron donation from cytosine to Ag(I), in accordance with HSAB theory.[38] In addition, the Ag 3d binding energies observed for HKUST-1-(Cyt)$_x$–Ag differed from those reported

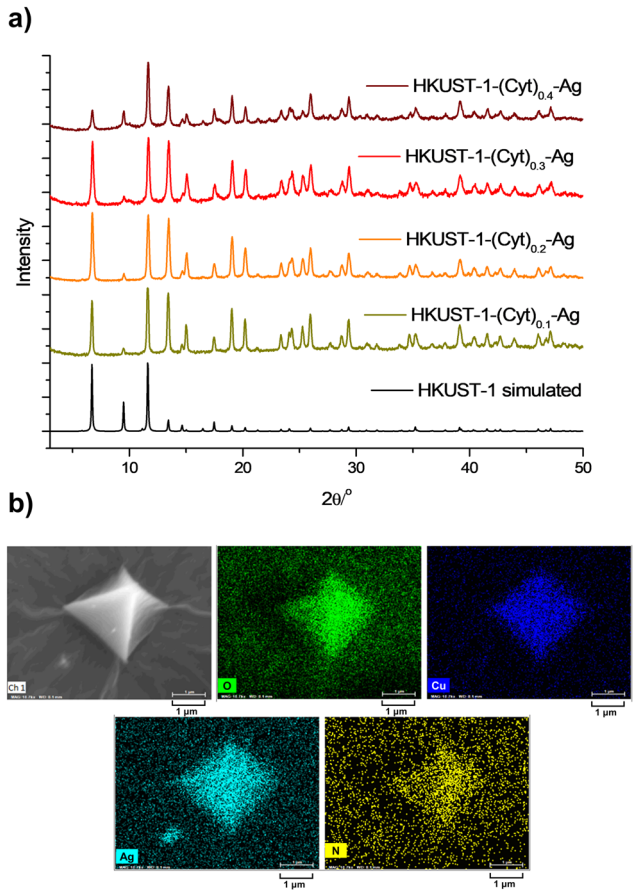

Fig. 3 Characterization data for HKUST-1-(Cyt)$_x$–Ag. (a) PXRD of HKUST-1-(Cyt)$_x$–Ag after metalation and (b) SEM-EDS mapping of HKUST-1-(Cyt)$_{0.3}$–Ag.

for Ag metal or Ag salts (Fig. S3 and Table S4), indicating a modified electronic environment arising from coordination between Ag and the N sites of cytosine.[39] Taken together, these XPS results provide strong evidence for the formation of Ag–cytosine coordination centers within HKUST-1-(Cyt)$_x$–Ag.

Laccase-mimicking reactions with HKUST-1-Cyt–Ag

Laccase is a multi-copper oxidase that catalyzes the oxidation of various aromatic substrates, including phenol derivatives, using molecular oxygen (O_2) as the terminal electron acceptor and producing water as the only byproduct. This eco-friendly pathway has been widely investigated for pollutant degradation.[21,40,41] Although laccase is generally regarded as a relatively stable oxidase under mild aqueous conditions, its catalytic activity often decreases in more demanding environments such as elevated temperatures, organic media, or repeated usage. As a result, limitations associated with operational stability, cost, and recyclability continue to restrict its use in practical and large-scale processes. To address these challenges, artificial nanozymes and MOF-based laccase mimics have been developed as more robust alternatives for designing durable catalytic systems. Consequently, these laccase-mimicking catalysts have emerged as promising nanozyme platforms capable of overcoming such drawbacks.[21,41–51]

As an initial study, the laccase-like activity of pristine HKUST-1 was examined under various pH conditions. In the absence of the MOF, the substrates 4-aminoantipyrine (4-AAP) and 2,4-dichlorophenol (2,4-DP) showed no UV absorbance between 400 and 600 nm. In contrast, catalytic reactions with HKUST-1 produced a clear absorption peak at 510 nm, corresponding to the oxidative coupling product, confirming its intrinsic laccase-mimicking activity. The activity was pH-dependent, with optimal performance observed at pH 7 (Fig. S4). In addition, the reaction time was optimized by monitoring product formation through *in situ* UV-vis spectroscopy for the HKUST-1-(Cyt)$_{0.3}$–Ag catalyst. The time-course profiles show a steady increase in absorbance, followed by a clear plateau, indicating that the reaction proceeds to near completion under the optimized conditions (Fig. S5).

The catalytic activities of HKUST-1-Cyt and HKUST-1-Cyt–Ag were then compared. While HKUST-1-Cyt showed minimal influence, HKUST-1-Cyt–Ag exhibited markedly enhanced activity (Fig. 4a). The activity of HKUST-1-Cyt–Ag increased with higher cytosine incorporation, which can be attributed to the greater likelihood of forming Cyt–Ag–Cyt units at higher cytosine site densities. These units act as the primary catalytic motifs in the system and therefore directly contribute to the observed improvement. However, when the cytosine incorporation reached 40 percent, the activity decreased, likely due to partial pore blocking and restricted substrate diffusion within the framework under aqueous conditions (Fig. S6). This finding suggests that excessive loading of Cyt–Ag species can lead to steric congestion or reduced accessibility of the active sites. Accordingly, the optimal cytosine incorporation ratio for HKUST-1-(Cyt)$_x$–Ag was determined to be approximately 30 percent.

Next, we sought to verify the difference in synergistic effects between the case where the Cyt–Ag complex was freely dispersed in solution and the case where it was immobilized within the pores of HKUST-1 (Fig. 4b). First, a homogeneous Cyt–Ag complex was synthesized so that it could freely diffuse under the reaction conditions. When used alone in aqueous solution, this Cyt–Ag complex showed only low catalytic activity. Interestingly, when the complex was simply mixed with HKUST-1 without immobilization, a moderate synergistic effect emerged and the activity exceeded that of pristine HKUST-1.

However, the HKUST-1-Cyt–Ag composite exhibited significantly higher activity than the physical mixture of HKUST-1 and the Cyt–Ag complex. This clearly indicates that the catalytic process is predominantly promoted within the heterogeneous MOF environment, where the confined pore space stabilizes and enhances the active sites. The role of the Cyt–Ag units inside the MOF can be interpreted as follows: within the pore channels, Cyt–Ag motifs may act as auxiliary redox-active centers that facilitate efficient electron transfer between the Cu nodes and the substrate. In addition, the presence of Ag may subtly modulate the electronic environment of the Cu paddle-

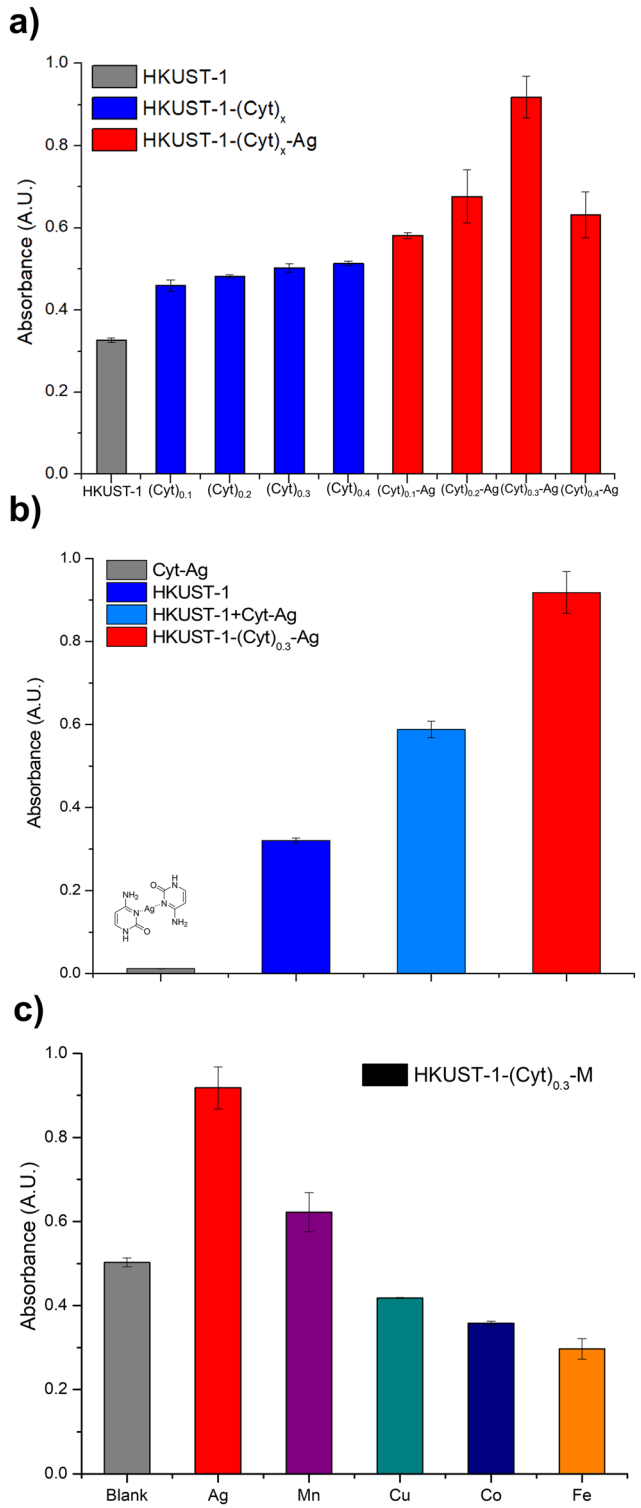

Fig. 4 (a) Catalytic activity for laccase-mimicking reactions with HKUST-1-Cyt and HKUST-1-(Cyt)$_x$–Ag, (b) comparison of the reactivity of the Cyt–Ag complex and HKUST-1-Cyt–Ag, and (c) metal screening of HKUST-1-(Cyt)$_{0.3}$–M (M = Ag, Mn, Cu, Co, and Fe). Screening metals were selected from those reported to exhibit laccase activity.

wheel nodes, providing a more favorable interface for substrate activation and redox cycling. It should be noted that HKUST-1 gradually decomposes in phosphate buffer; therefore, at extended reaction times, a minor homogeneous contribution from leached Cyt–Ag species may arise. Nevertheless, this solution-phase activity remains significantly lower than that of the intact HKUST-1-(Cyt)$_{0.3}$–Ag composite and cannot account for the high initial reaction rates.

To evaluate the effect of different metals, HKUST-1-(Cyt)$_{0.3}$–M (M = Ag, Mn, Cu, Co, Fe) was examined (Fig. 4c and S7). Although Mn incorporation led to improved activity compared to Cu and Fe, Ag provided the highest catalytic efficiency in the oxidative coupling of 4-AAP and 2,4-DP. This can be attributed to the strong HSAB interaction between the soft basic binding site of cytosine and the soft Lewis acid Ag, which allows more abundant and stable Cyt–M coordination sites to form compared to harder or borderline metal ions. These richer Cyt–Ag motifs can therefore work synergistically with the Cu nodes to yield a more efficient catalytic system.[38]

Lastly, the kinetic parameters of the laccase-mimicking reaction were determined using the Michaelis–Menten equation to quantitatively evaluate the catalytic performance of HKUST-1-Cyt–Ag. The general calculation method followed previous reports (see the SI for details).[49,51] Specifically, the values of K_m and V_{max} were obtained and compared with literature data (Fig. S8 and Table 1). The results revealed that HKUST-1-(Cyt)$_{0.3}$–Ag exhibited a V_{max} approximately 4.5-fold higher than that of pristine HKUST-1.

This enhancement is likely attributed to the strong oxidation-promoting activity of the Cyt–Ag moiety, which facilitates efficient substrate oxidation. Previous literature has reported that systems incorporating multi-copper centers or functionalized ligands can diversify catalytically active sites,[42,47] thereby achieving high V_{max} values despite exhibiting substrate affinities comparable to those of natural laccase. However, in this MOF system, in addition to the Cu cluster, the incorporation of the Cyt–Ag motif introduces an additional cooperative active center that operates in concert with the Cu paddlewheel clusters. This dual-site configuration not only enhances reactivity but also results in a marked improvement in substrate affinity, as reflected by the substantial decrease in K_m. Unlike pristine HKUST-1, which contains only mononuclear Cu^{2+} paddlewheel clusters, the incorporation of the Cyt–Ag motif enables the formation of multiple synergistic active sites and pore environment engineering within the framework. This combined synergy affords an approximately 4.5-fold enhancement in V_{max} relative to pristine HKUST-1, placing HKUST-1-(Cyt)$_{0.3}$–Ag among the more strongly activated laccase-mimicking platforms in comparison with representative systems summarized in Table 1, while simultaneously improving substrate affinity.

Based on the ICP-OES data, HKUST-1-(Cyt)$_x$–Ag showed a clear trend: higher Ag content within the MOF generally led to greater reactivity. The H$_2$*m*BDC ligand has fewer coordination sites than H$_3$BTC, so its incorporation creates structural defects in the framework. When the proportion of H$_2$*m*BDC is

Table 1 Kinetic parameters of laccase-mimicking reactions (2,4-DP + 4-AAP) with various heterogeneous catalysts

Catalyst	K_m (mM)	V_{max} ($\times 10^{-3}$ mM min^{-1})	Pristine catalyst/ natural enzyme	K_m (mM)	V_{max} ($\times 10^{-3}$ mM min^{-1})	Ref.
HKUST-1-(Cyt)$_{0.1}$–Ag	0.033	0.38	HKUST-1	0.36	0.22	This work
HKUST-1-(Cyt)$_{0.2}$–Ag	0.086	0.65				This work
HKUST-1-(Cyt)$_{0.3}$–Ag	**0.072**	**0.98**				This work
HKUST-1-(Cyt)$_{0.4}$–Ag	0.038	0.66				This work
Cu-SM MOF	0.073	—[a]	HKUST-1	0.116	—[a]	47
			Laccase	0.65	—[a]	
Cu/H_3BTC MOF	0.068	94	Laccase	0.062	5.8	41
Cu/GMP	0.59	830	Laccase	0.65	150	42
Cysteine–Histidine + Cu(II)	0.42	7.32	Laccase	0.41	6.41	49

[a] Not reported in the cited reference under the relevant experimental conditions.

moderate, these defects can facilitate Ag incorporation and improve activity. However, excessive defects negatively affect the structural integrity of the MOF. At the highest Ag loading, HKUST-1-(Cyt)$_{0.4}$–Ag, the catalytic activity decreased, likely due to partial collapse of the MOF structure caused by abundant defect sites, a phenomenon commonly observed in MOF-catalyzed systems (Table S2 and Fig. 3a).[52,53] Therefore, HKUST-1-(Cyt)$_{0.3}$–Ag is regarded as the optimized MOF in this system.

This high reactivity was also reproduced in the oxidation of a single chromogenic substrate, epinephrine. Michaelis–Menten analysis of the adenochrome formation reaction confirmed that HKUST-1-(Cyt)$_{0.3}$–Ag exhibits a markedly higher V_{max} than pristine HKUST-1 as well as several reported laccase-mimicking systems (Fig. S9 and Table S5). These results validate that the catalytic efficiency of HKUST-1-(Cyt)$_{0.3}$–Ag is not limited to the 2,4-DP/4-AAP assay but extends to single-substrate laccase probes. The corresponding kinetic parameters are summarized in Table S5.

Although the HKUST-1-Cyt–Ag catalyst exhibited excellent laccase-mimicking activity under the MOF nanozyme concept, the optimized reaction conditions were not fully compatible with the HKUST-1 framework. HKUST-1 is known to exhibit poor hydrolytic stability in aqueous media due to competitive coordination,[54,55] and its stability further decreases under basic aqueous conditions.[25] In this study, both pristine HKUST-1 and HKUST-1-Cyt–Ag completely dissolved in pH 7 buffer within 1 hour, as evidenced by the disappearance of all HKUST-1 diffraction peaks and the absence of any remaining solid material after incubation (Fig. S10).

To mitigate structural decomposition, DMF was added as an additive following a reported strategy to protect the open metal sites of Cu in HKUST-1, thereby improving framework stability.[56] The coordinating ability of DMF blocks competitive ligand exchange with water, slowing hydrolytic degradation, and partial retention of PXRD intensity was observed when a small amount of DMF was added (Fig. S10). However, although DMF delayed the onset of framework collapse, the catalytic activity was not fully preserved. Thus, while addition of an SBU-protecting solvent such as DMF can improve the structural stability of HKUST-1-Cyt–Ag during reuse, this stabilization occurs at the cost of reduced reactivity.

Conclusions

In this study, a catalytically active Cyt–Ag complex was incorporated into a Cu-based MOF framework using a mixed-ligand strategy. Cyt was introduced *via* a pre-synthesized H_2mBDC-Cyt ligand, and Ag(I) ions were anchored to the Cyt moiety through post-synthetic metalation. Crystallinity was preserved while controlling the functional ligand content, with 30 mol% H_2mBDC-Cyt (HKUST-1-(Cyt)$_{0.3}$) identified as the optimal ratio. This composition enabled efficient Ag loading without introducing excessive structural defects arising from the lower coordination number of H_2mBDC compared to H_3BTC.

HKUST-1-(Cyt)$_{0.3}$–Ag exhibited synergistic reactivity from both the Cu(II) cluster and Cyt–Ag complex in laccase-mimicking oxidative coupling of phenols. Michaelis–Menten analysis revealed an approximately 4.5-fold increase in V_{max} compared to pristine HKUST-1, underscoring the catalytic role of the Cyt–Ag motif. ICP-OES confirmed that Ag content increased with higher Cyt loading; however, excessive incorporation generated abundant defect sites and reduced performance, as observed for HKUST-1-(Cyt)$_{0.4}$–Ag, where partial framework collapse was likely responsible for the decline.

Despite its high activity, HKUST-1-(Cyt)$_{0.3}$–Ag showed poor hydrolytic stability, decomposing in pH 7 buffer within 1 h. Addition of DMF, following a reported strategy to protect open Cu sites in the SBUs, partially preserved crystallinity but did not maintain full catalytic activity. Overall, these findings demonstrate that Cyt–Ag incorporation into MOFs can effectively enhance nanozyme performance through synergistic metal–ligand interactions and controlled defect engineering. Future work will focus on improving aqueous stability through linker hydrophobicity tuning, node-protecting ligands, and alternative MOF topologies, thereby enabling broader applications in biosensing, environmental remediation, and selective oxidation catalysis.

Author contributions

Jonghyeon Lee: writing – original draft, methodology, investigation, and data curation. Gahyeon Baek: methodology and data

curation. Youngjo Kim: funding acquisition and supervision. Soyoung Park: conceptualization, supervision, data curation, funding acquisition, and writing – original draft. Min Kim: conceptualization, supervision, data curation, funding acquisition, project administration, and writing – original draft.

Conflicts of interest

There are no conflicts to declare.

Data availability

The data supporting this article have been included as part of Supplementary Information (SI), which contains detailed experimental procedures, characterization data, catalytic assays, kinetic analysis, and additional figures and tables. Supplementary information is available. See DOI: https://doi.org/10.1039/d5dt02837j.

Acknowledgements

This research was supported by the Basic Science Research Program through the National Research Foundation of Korea (NRF) funded by the Ministry of Science and ICT (RS-2024-00352112). Y. Kim gratefully acknowledges financial support from the academic research program of Chungbuk National University in 2025. S. Park would like to acknowledge the 'Rising Fellow Program' from Toyota Physical and Chemical Research Institute. In addition, J. Lee is financially supported by the NRF funded by the Ministry of Science and ICT (PhD student research fellowship, RS-2025-25414073).

References

1 F. Pu, J. Ren and X. Qu, *Chem. Soc. Rev.*, 2018, **47**, 1285–1306.
2 S. Sivakova and S. J. Rowan, *Chem. Soc. Rev.*, 2005, **34**, 9–21.
3 K. Chen, Z. Du, Y. Zhang, R. Bai, L. Zhu and W. Xu, *Biosensors*, 2025, **15**, 142.
4 Z. Khademi and K. Nikoofar, *RSC Adv.*, 2025, **15**, 3192–3218.
5 Y. Rachuri, J. F. Kurisingal, R. K. Chitumalla, S. Vuppala, Y. Gu, J. Jang, Y. Choe, E. Suresh and D. W. Park, *Inorg. Chem.*, 2019, **58**, 11389–11403.
6 N. Li, J. Liu, J. J. Liu, L. Z. Dong, Z. F. Xin, Y. L. Teng and Y. Q. Lan, *Angew. Chem., Int. Ed.*, 2019, **58**, 5226–5231.
7 F. Gholamian and M. Hajjami, *Polyhedron*, 2019, **170**, 649–658.
8 M. Nikoorazm, B. Tahmasbi, S. Gholami and P. Moradi, *Appl. Organomet. Chem.*, 2020, **34**, e5919.
9 S. Park, L. Zheng, S. Kumakiri, S. Sakashita, H. Otomo, K. Ikehata and H. Sugiyama, *ACS Catal.*, 2014, **4**, 4070–4073.
10 S. Park, I. Okamura, S. Sakashita, J. H. Yum, C. Acharya, L. Gao and H. Sugiyama, *ACS Catal.*, 2015, **5**, 4708–4712.
11 A. Ono, S. Cao, H. Togashi, M. Tashiro, T. Fujimoto, T. Machinami, S. Oda, Y. Miyake, I. Okamoto and Y. Tanaka, *Chem. Commun.*, 2008, 4825–4827.
12 J. Kondo, Y. Tada, T. Dairaku, Y. Hattori, H. Saneyoshi, A. Ono and Y. Tanaka, *Nat. Chem.*, 2017, **9**, 956–960.
13 H. A. Day, C. Huguin and Z. A. Waller, *Chem. Commun.*, 2013, **49**, 7696–7698.
14 X. Dong, Z. Qiu, Z. Wang, J. Li, W. Qin, J. Dang, W. Zhou, G. Jia, Y. Chen and C. Wang, *Angew. Chem., Int. Ed.*, 2024, **63**, e202407838.
15 T. Dairaku, K. Nozawa-Kumada, T. Ono, K. Yoshida, Y. Kashiwagi, Y. Tanaka, J. Kondo and M. Tanabe, *Inorg. Chem.*, 2024, **63**, 22845–22855.
16 C. Sun, X.-L. Liu, S.-J. Xiao, Q. Shi, Z.-H. Xue, Y.-T. Luo, R.-P. Liang, L. Zhang and J.-D. Qiu, *Chem. Eng. Sci.*, 2025, **314**, 121812.
17 L. Capdevila, E. Andris, A. Briš, M. Tarrés, S. Roldán-Gómez, J. Roithová and X. Ribas, *ACS Catal.*, 2018, **8**, 10430–10436.
18 J. A. Flores, N. Komine, K. Pal, B. Pinter, M. Pink, C.-H. Chen, K. G. Caulton and D. J. Mindiola, *ACS Catal.*, 2012, **2**, 2066–2078.
19 A. Tlahuext-Aca and J. F. Hartwig, *ACS Catal.*, 2021, **11**, 1119–1127.
20 Z. Xu, C. Zhang, X. Wang and D. Liu, *ACS Appl. Bio Mater.*, 2021, **4**, 3985–3999.
21 A. Koyappayil, H. T. Kim and M. H. Lee, *J. Hazard. Mater.*, 2021, **412**, 125211.
22 D. H. Hong, H. S. Shim, J. Ha and H. R. Moon, *Bull. Korean Chem. Soc.*, 2021, **42**, 956–969.
23 J. F. Kurisingal, J. H. Choe, H. Kim, J. Youn, G. Cheon and C. S. Hong, *Bull. Korean Chem. Soc.*, 2024, **45**, 675–688.
24 S. Jeong and H. R. Moon, *Bull. Korean Chem. Soc.*, 2024, **45**, 308–316.
25 J. Y. Kim, J. Kang, S. Cha, H. Kim, D. Kim, H. Kang, I. Choi and M. Kim, *Nanomaterials*, 2024, **14**, 110.
26 J. Kang, S. Cha, J. Ryu, B. An, C. Lim, Y. Heo, I. Choi and M. Kim, *Bull. Korean Chem. Soc.*, 2025, **46**, 231–252.
27 S. L. Anderson and K. C. Stylianou, *Coord. Chem. Rev.*, 2017, **349**, 102–128.
28 B. Liu, M. Jiang, D. Zhu, J. Zhang and G. Wei, *Chem. Eng. J.*, 2022, **428**, 131118.
29 Z. Zhang, Y. Li, Z. Yuan, L. Wu, J. Ma, W. Tan, Y. Sun, G. Zhang and H. Chai, *Inorg. Chem. Front.*, 2025, **12**, 400–429.
30 W. Xu, Y. Wu, W. Gu, D. Du, Y. Lin and C. Zhu, *Chem. Soc. Rev.*, 2024, **53**, 137–162.
31 S. S.-Y. Chui, S. M.-F. Lo, J. P. H. Charmant, A. G. Orpen and I. D. Williams, *Science*, 1999, **283**, 1148–1150.
32 C. H. Hendon and A. Walsh, *Chem. Sci.*, 2015, **6**, 3674–3683.
33 M. Kabir, M. Rahman, T. Islam, Q. Meng, H. Liu, M. Li and S. Wu, *Chem. Eng. J.*, 2025, **513**, 162753.
34 S. H. Park, H. M. Kim, M. L. Diaz-Ramirez, S. Lee and N. C. Jeong, *Chem. Commun.*, 2024, **60**, 14577–14580.

35 D. Sharma, S. Rasaily, S. Pradhan, K. Baruah, S. Tamang and A. Pariyar, *Inorg. Chem.*, 2021, **60**, 7794–7802.
36 Y. P. Budiman, M. Rashifari, S. Azid, I. Z. Ghafara, Y. Deawati, Y. Permana, U. S. F. Arrozi, W. Ciptonugroho, T. Mayanti and W. W. Lestari, *ChemistrySelect*, 2024, **9**, e202304913.
37 G. W. Peterson, K. Au, T. M. Tovar and T. H. Epps, *Chem. Mater.*, 2019, **31**, 8459–8465.
38 M. Kohagen, F. Uhlig and J. Smiatek, *Int. J. Quantum Chem.*, 2019, **119**, e25933.
39 M. Schreiber and L. Gonzalez, *J. Comput. Chem.*, 2007, **28**, 2299–2308.
40 D. M. Mate and M. Alcalde, *Biotechnol. Adv.*, 2015, **33**, 25–40.
41 S. Shams, W. Ahmad, A. H. Memon, Y. Wei, Q. Yuan and H. Liang, *RSC Adv.*, 2019, **9**, 40845–40854.
42 H. Liang, F. Lin, Z. Zhang, B. Liu, S. Jiang, Q. Yuan and J. Liu, *ACS Appl. Mater. Interfaces*, 2017, **9**, 1352–1360.
43 C. Y. Hu, Z. W. Jiang, C. Z. Huang and Y. F. Li, *Mikrochim. Acta*, 2021, **188**, 272.
44 T. N. Le, X. A. Le, T. D. Tran, K. J. Lee and M. I. Kim, *J. Nanobiotechnol.*, 2022, **20**, 358.
45 C. Liu, X. Zhang, Y. Zhou, L. Zhu, C. Zhang, X. Yan, S. You, W. Qi and R. Su, *Biochem. Eng. J.*, 2023, **194**, 108897.
46 X. Liu, P. An, Y. Han, H. Meng and X. Zhang, *Microchem. J.*, 2024, **201**, 110559.
47 B. Wang, P. Liu, Y. Hu, H. Zhao, L. Zheng and Q. Cao, *Dalton Trans.*, 2023, **52**, 2309–2316.
48 R. Zhang, L. Wang, J. Han, J. Wu, C. Li, L. Ni and Y. Wang, *J. Hazard. Mater.*, 2020, **383**, 121130.
49 J. Wang, R. Huang, W. Qi, R. Su, B. P. Binks and Z. He, *Appl. Catal., B*, 2019, **254**, 452–462.
50 J. Wang, R. Huang, W. Qi, R. Su and Z. He, *Chem. Eng. J.*, 2022, **434**, 134677.
51 J. H. Yum, T. Kumagai, D. Hori, H. Sugiyama and S. Park, *Nanoscale*, 2023, **15**, 10749–10754.
52 Y. Shan, G. Zhang, Y. Shi and H. Pang, *Cell Rep. Phys. Sci.*, 2023, **4**, 101301.
53 D. Bůžek, J. Hynek, M. Kloda, V. Zlámalová, P. Bezdička, S. Adamec, K. Lang and J. Demel, *Inorg. Chem. Front.*, 2024, **11**, 5319–5335.
54 M. Todaro, G. Buscarino, L. Sciortino, A. Alessi, F. Messina, M. Taddei, M. Ranocchiari, M. Cannas and F. M. Gelardi, *J. Phys. Chem. C*, 2016, **120**, 12879–12889.
55 J. R. Alvarez, E. Sanchez-Gonzalez, E. Perez, E. Schneider-Revueltas, A. Martinez, A. Tejeda-Cruz, A. Islas-Jacome, E. Gonzalez-Zamora and I. A. Ibarra, *Dalton Trans.*, 2017, **46**, 9192–9200.
56 J. Bae, J. S. Choi, S. Hwang, W. S. Yun, D. Song, J. Lee and N. C. Jeong, *ACS Appl. Mater. Interfaces*, 2017, **9**, 24743–24752.